Supporting Information

Breaking sodium solubility limit for extraordinary thermoelectric performance in p-type PbTe

Yingcai Zhu, [a] Lei Hu, [b] Shaoping Zhan, [a] Toshiaki Ina, [c] Xiang Gao, [d] Tao Hong [a, *] and Li-Dong Zhao [a, *]

[a] School of Materials Science and Engineering, Beihang University, Beijing 100191, China

[b] State Key Laboratory for Mechanical Behavior of Materials, Xi'an Jiaotong University, Xi'an 710049, China

[c] Research and Utilization Division, Japan Synchrotron Radiation Research Institute (JASRI/SPring-8), Sayo, Hyogo, Japan

[d] Center for High Pressure Science and Technology Advanced Research (HPSTAR), Beijing, 100094, China

[*] hongtao77@buaa.edu.cn
[*] zhaolidong@buaa.edu.cn (L.-D. Zhao)

X-ray absorption fine structure (XAFS) spectra measurements. We conducted the XAFS experiments at the BL01B1 beamline of Spring-8 in Japan. The storage ring runs in top-up mode with an accumulated current of 99.5 mA during the experiment. The Si (311) double-crystal monochromator was used for modulating the energy of beam. The XAFS spectra of Ag *K*-edge for $AgInSe_2$ and $AgInTe_2$ were measured in transmission mode. The Ag *K*-edge and Se *K*-edge XAFS spectra for $Pb_{0.98}Na_{0.02}Te$-0.5% $AgInSe_2$ were performed in fluorescence mode using a 19-element Ge solid-state detector (SSD). The Se *K*-edge XAFS spectrum of PbSe and the Te *K*-edge and Pb L_3-edge XAFS spectra for PbTe and $Pb_{0.98}Na_{0.02}Te$-0.5% $AgInSe_2$ were conducted in transmission mode. All experimental XAFS spectra were processed using the IFFEFIT package.[1]

X-ray absorption near edge structure (XANES) calculation. The XANES spectrum calculation of Se *K*-edge was conducted based on the full multiple scattering (FMS) theory using FEFF9 program[2, 3] assuming Se atoms occupy the Te sites in PbTe matrix. Self-consistent field (SCF) method was used to estimate the atomic scattering potential. We only replace the central Te absorber with Se atom and maintain the coordination in PbTe matrix due to the small doping content of Se atoms. The cluster radius for SCF and FMS were fixed as 8 and 10 Angstrom, respectively, and this is enough to achieve good convergence for this calculation.

Transport properties estimation using SPB model. The following equations were used to estimate the Pisarenko relationship, carrier mobility, Lorenz number, and optimum *ZT* value:[4, 5]

$$S = \frac{k_B}{e}\left(\frac{2F_1(\eta)}{F_0(\eta)} - \eta\right) \tag{S1}$$

$$n = 4\pi\left(\frac{2m^* k_B T}{h^2}\right)^{3/2} F_{1/2}(\eta) \tag{S2}$$

$$r_H = \frac{3F_{1/2}(\eta)\,F_{-1/2}(\eta)}{4\quad F_0^2(\eta)} \tag{S3}$$

$$\mu_H = \frac{e\qquad \pi\hbar^4 v_L^2 \rho\qquad F_{-1/2}(\eta)}{m^*\sqrt{2}E_{def}^2\left(m^* k_B T\right)^{3/2}\quad 2F_0(\eta)} \tag{S4}$$

$$|E_{def}| = \left(\frac{hk_B^2\quad v_L^2 \rho T}{3\pi^2 m^* \kappa_L B}\right)^{1/2} \tag{S5}$$

$$B = \left(\frac{k_B}{e}\right)^2 \frac{\sigma_{E_0} T}{\kappa_L} \tag{S6}$$

$$\sigma_{E_0} = \sigma / F_0(\eta) \tag{S7}$$

$$L = \frac{k_B^2}{e^2}\left(\frac{3F_0(\eta)F_2(\eta) - 4F_1{}^2(\eta)}{F_0{}^2(\eta)}\right) \tag{S8}$$

$$ZT = \frac{S^2(\eta)}{\frac{(k_B/e)^2}{B \ln\left(1 + e^{\eta}\right)} + L(\eta)} \tag{S9}$$

Here, k_B is the Boltzmann constant, e is the electron charge, F_j is the Fermi-Dirac integral ($F_j(\eta) = \int_0^{\infty} \frac{\xi^j d\xi}{1 + exp(\xi - \eta)}$), and η is the reduced Fermi level E_F/k_BT, m^* is the effective mass, h is the Plank constant, v_L is the longitudinal sound velocity, ρ is the density of sample, E_{def} is the deformation potential. The effective mass (m^*) will be determined with experimental n_H and Seebeck coefficient using equation S1-S3. The Hall carrier concentration (n_H) is related to n via $n_H = n/r_H$. Both Seebeck coefficient and Hall factor (r_H) are only a function of the reduced Fermi level (η). For a given effective mass, various Seebeck coefficient (S) and Hall carrier concentration (n_H) can be obtained with varying η and thus we get the theoretical S - n_H plot (Pisarenko line). Similarly, the relation between μ_H and n_H can be calculated using equation (S1-S7). The Lorenz number (L) was estimated using equation S8 assuming acoustic-phonon scattering dominates. The ZT value as a function of reduced Fermi level (η) was calculated using equations S6-S9.

Two-band model simulation

Considering two valence bands (L and Σ) participate in the transport process, the Seebeck coefficient can be expressed as:[4]

$$S = (S_L\sigma_L + S_\Sigma\sigma_\Sigma)/(\sigma_L + \sigma_\Sigma) \tag{S10}$$

To simplify, we assume these two valence bands as single parabolic bands. Thus, the Seebeck coefficients and electrical conductivities contributed from each band can be determined using following equations:

$$S_L = \frac{k_B}{e}\left(\frac{2F_1(\eta_1)}{F_0(\eta_1)} - \eta_1\right) \tag{S11}$$

$$S_{\Sigma} = \frac{k_B}{e}\left(\frac{2F_1(\eta_2)}{F_0(\eta_2)} - \eta_2\right) \quad \text{(S12)}$$

$$\sigma_L = n_{H1} e \mu_{H1} \quad \text{(S13)}$$

$$\sigma_{\Sigma} = n_{H2} e \mu_{H2} \quad \text{S14)}$$

$$n_{H1} = \frac{n}{r_{H1}} = 4\pi\left(\frac{2m_L^* k_B T}{h^2}\right)^{3/2} F_{1/2}(\eta_1)/r_{H1} \quad \text{(S15)}$$

$$n_{H2} = \frac{n}{r_{H2}} = 4\pi\left(\frac{2m_{\Sigma}^* k_B T}{h^2}\right)^{3/2} F_{1/2}(\eta_2)/r_{H2} \quad \text{(S16)}$$

$$\mu_{H1} = \frac{e}{m_L^* \sqrt{2} E_{def1}^2 \left(m_L^* k_B T\right)^{3/2}} \frac{\pi \hbar^4 v_L^2 \rho}{2F_0(\eta_1)} \frac{F_{-1/2}(\eta_1)}{} \quad \text{(S17)}$$

$$\mu_{H2} = \frac{e}{m_{\Sigma}^* \sqrt{2} E_{def2}^2 \left(m_{\Sigma}^* k_B T\right)^{3/2}} \frac{\pi \hbar^4 v_L^2 \rho}{2F_0(\eta_2)} \frac{F_{-1/2}(\eta_2)}{} \quad \text{(S18)}$$

The total Hall carrier concentration (n_H) can be obtained via:

$$n_H = n_{H1} + n_{H2} \quad \text{(S19)}$$

The relation between η_1 and η_2 can be expressed as:

$$\eta_2 = \eta_1 - E_{off}/k_B T \quad \text{(S20)}$$

where the E_{off} represents the band offset between valence band L and Σ. The Seebeck coefficient (S) as a function of Hall carrier concentration can be estimated with varying η_1 when the parameters m_L^*, m_{Σ}^*, E_{def1}, E_{def2} and E_{off} are given. The room-temperature effective mass m_L^* and m_{Σ}^* were reported to be ~ 0.36 m_e and ~ 2 m_e, respectively.[6-8] In SPB model, the effective mass (m*) of $Pb_{0.99}Na_{0.01}Te$ - 0.5% $AgInSe_2$ is ~ 0.8 m_e. The deviation behavior in the Pisarenko plot (Figure 6a) indicate multiple valence band effects. Here, we simply set m_L^* as 0.8 m_e and estimate the S - n_H relation considering the effect of secondary valence band (Σ) with m_{Σ}^* = 2 m_e. We can get a good simulation (red line in **Figure 7**(a)) when E_{def1} = 19 eV, E_{def2} = 7 eV, and E_{off} = 0.18 eV, which is well consistent with the experimental results. Previous studies show that the deformation potential for L band and Σ band are ~ 19 eV and ~ 9.5 eV, respectively.[8, 9] The band offset between L band and Σ band (E_{off}) is ~ 0.15-0.2 eV.[10, 11] Therefore, the parameters we used are reasonable.

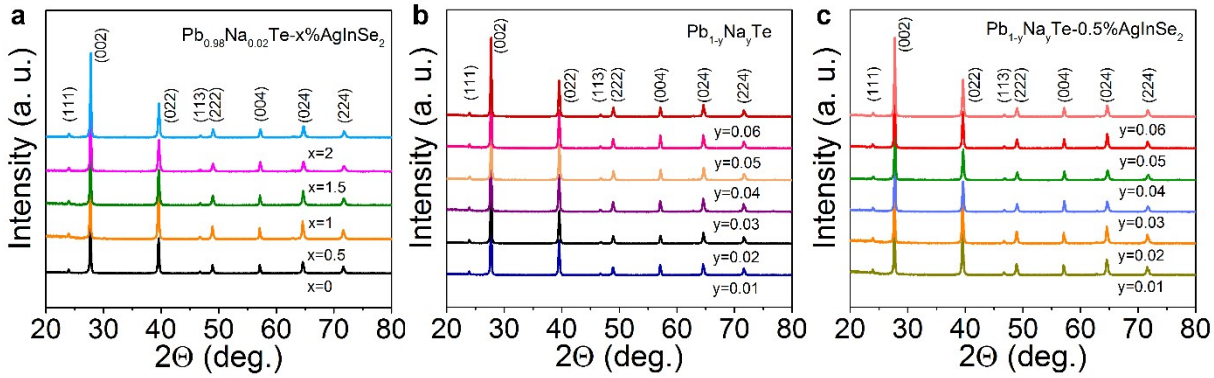

Figure S1. X-ray diffraction patterns for (a) $Pb_{0.98}Na_{0.02}Te$ - *x*% $AgInSe_2$, (b) $Pb_{0.98}Na_{0.02}Te$, and (c) $Pb_{1-y}Na_yTe$ - 0.5% $AgInSe_2$ samples.

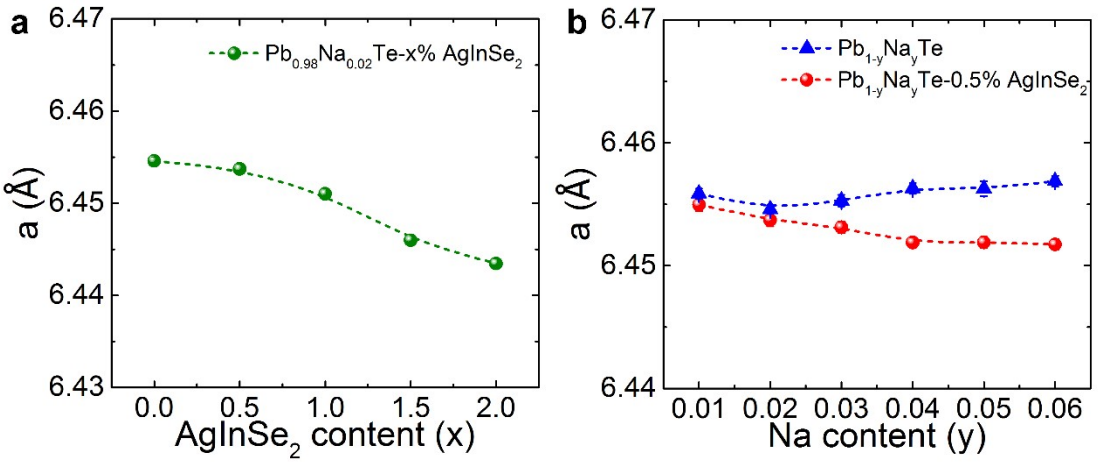

Figure S2. The lattice parameter for (a) $Pb_{0.98}Na_{0.02}Te$ - *x*% $AgInSe_2$, (b) $Pb_{0.98}Na_{0.02}Te$, and $Pb_{1-y}Na_yTe$ - 0.5% $AgInSe_2$ samples.

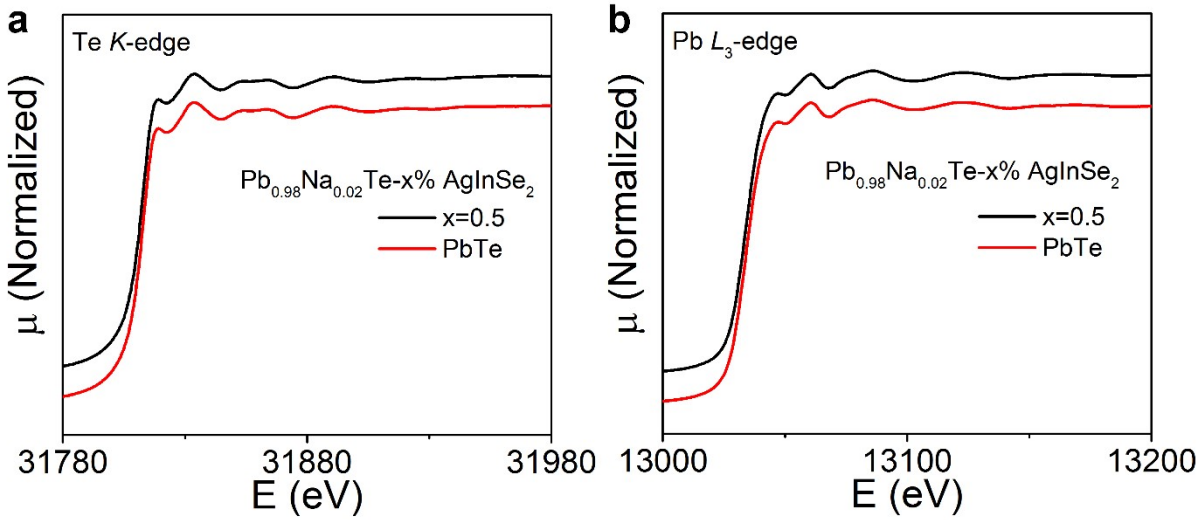

Figure S3. Experimental XANES spectra at (a) Te *K*-edge and (b) Pb L_3-edge for $Pb_{0.98}Na_{0.02}Te$ - 0.5%$AgInSe_2$ (black line), PbTe (red line), respectively.

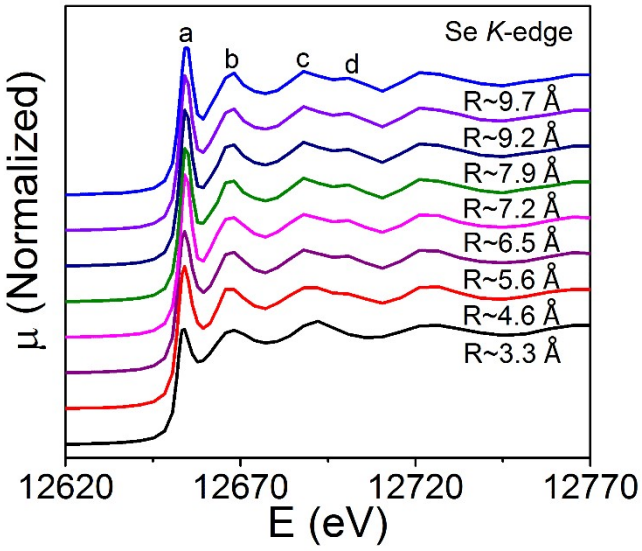

Figure S4. The calculated Se *K*-edge XANES spectra as a function of the cluster size assuming that Se occupies Te site in PbTe matrix.

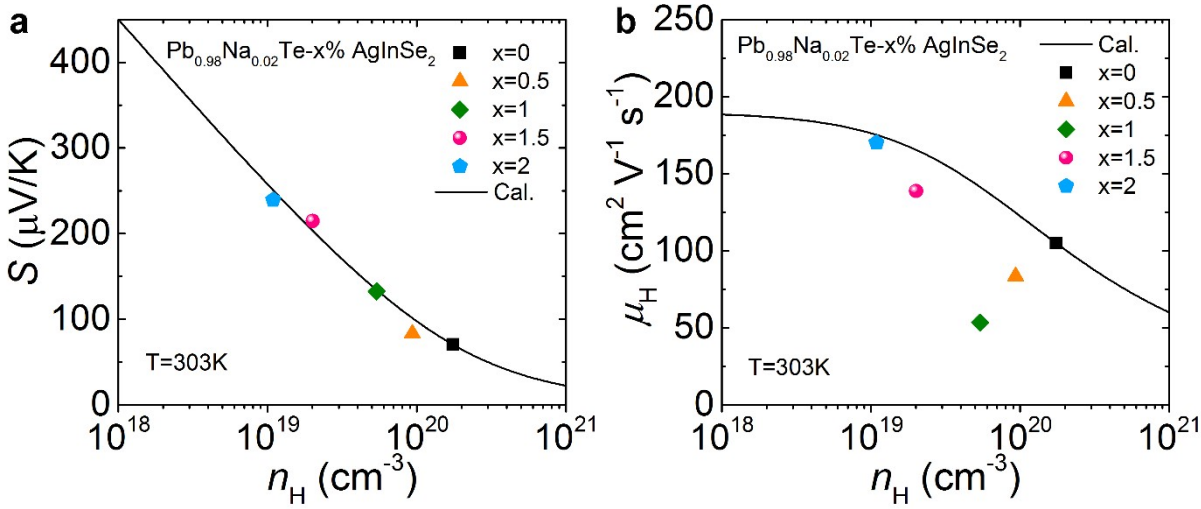

Figure S5. (a) The Seebeck coefficients as a function of Hall carrier concentration (Pisarenko plot) for $Pb_{0.98}Na_{0.02}Te$ - *x*% $AgInSe_2$ at room temperature. (b) The Hall carrier mobility versus Hall carrier concentration for $Pb_{0.98}Na_{0.02}Te$ - *x*% $AgInSe_2$ at room temperature. The solid lines represent calculated results using SPB model.

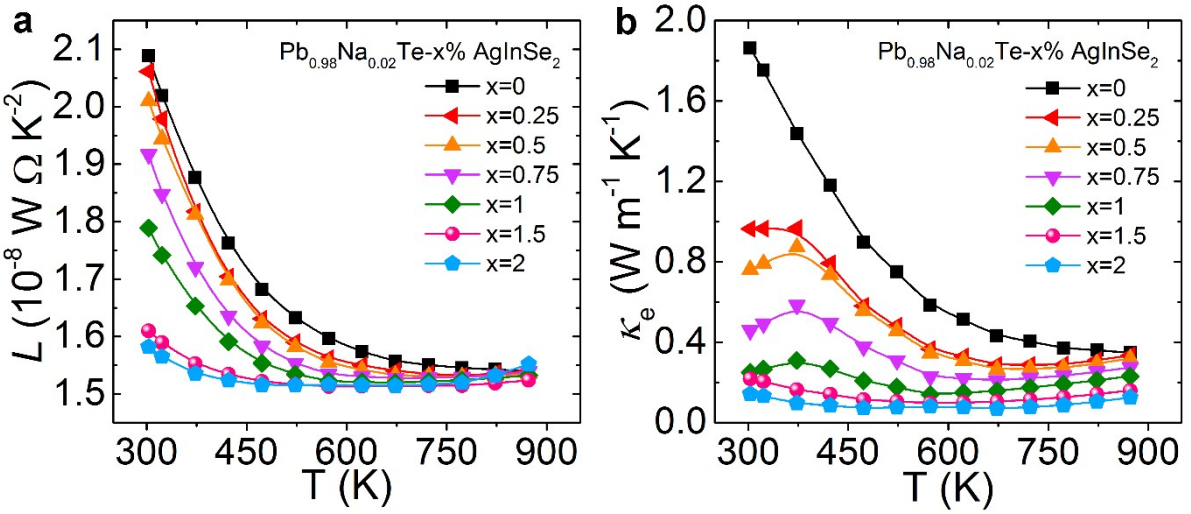

Figure S6. Temperature-dependent (a) Lorenz number and (b) electrical thermal conductivity for $Pb_{0.98}Na_{0.02}Te$ - *x*% $AgInSe_2$ compounds.

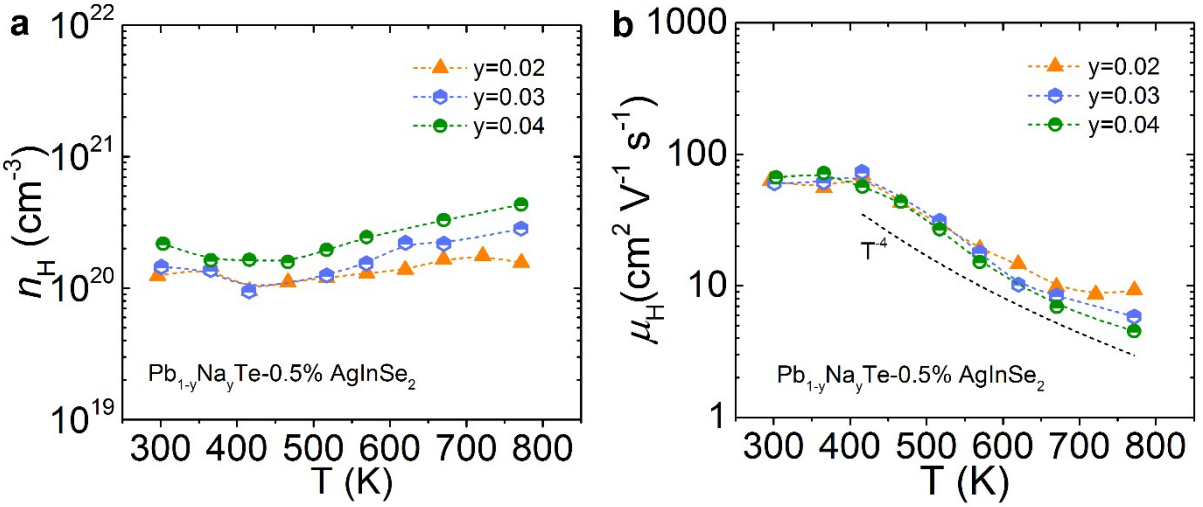

Figure S7. Temperature-dependent (a) Hall carrier concentration and (b) Hall carrier mobility for $Pb_{1-y}Na_yTe$-0.5% $AgInSe_2$.

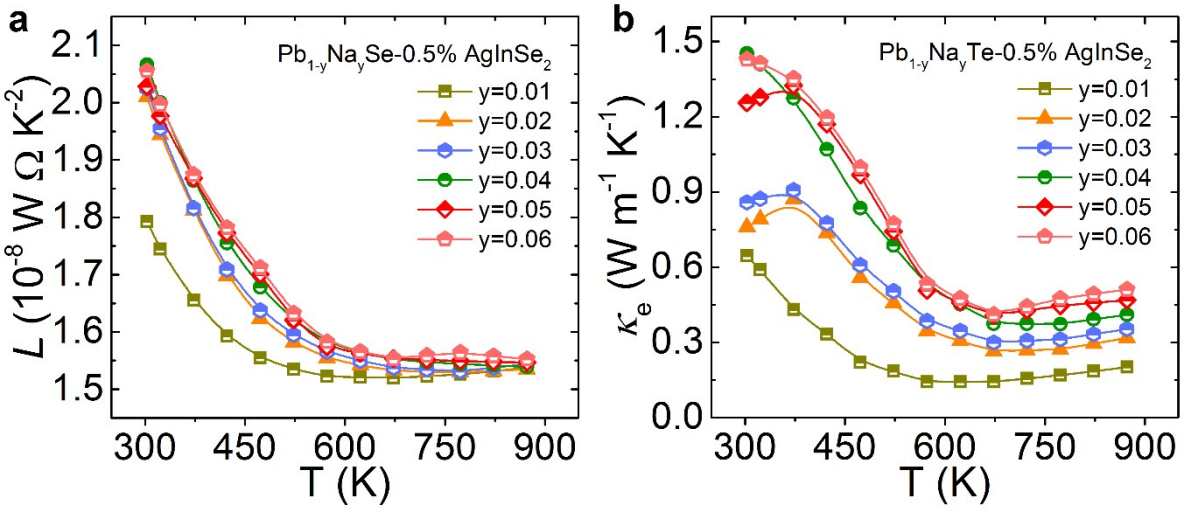

Figure S8. Temperature-dependent (a) Lorenz number and (b) electrical thermal conductivity for $Pb_{1-y}Na_yTe$ - 0.5% $AgInSe_2$ compounds.

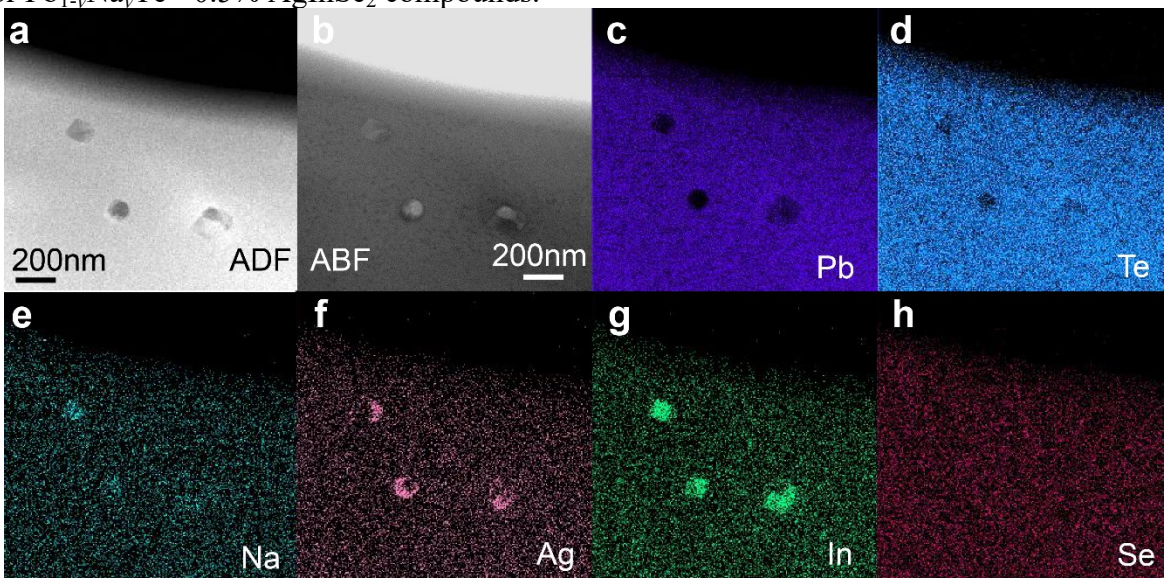

Figure S9. The (a) ADF and (b) ABF images of $Pb_{0.95}Na_{0.05}Te$-0.5%$AgInSe_2$ sample and the corresponding energy dispersive X-ray spectroscopy (EDS) mappings of (c) Pb, (d)Te, (e)Na, (f) Ag, (g) In, and (h) Se.

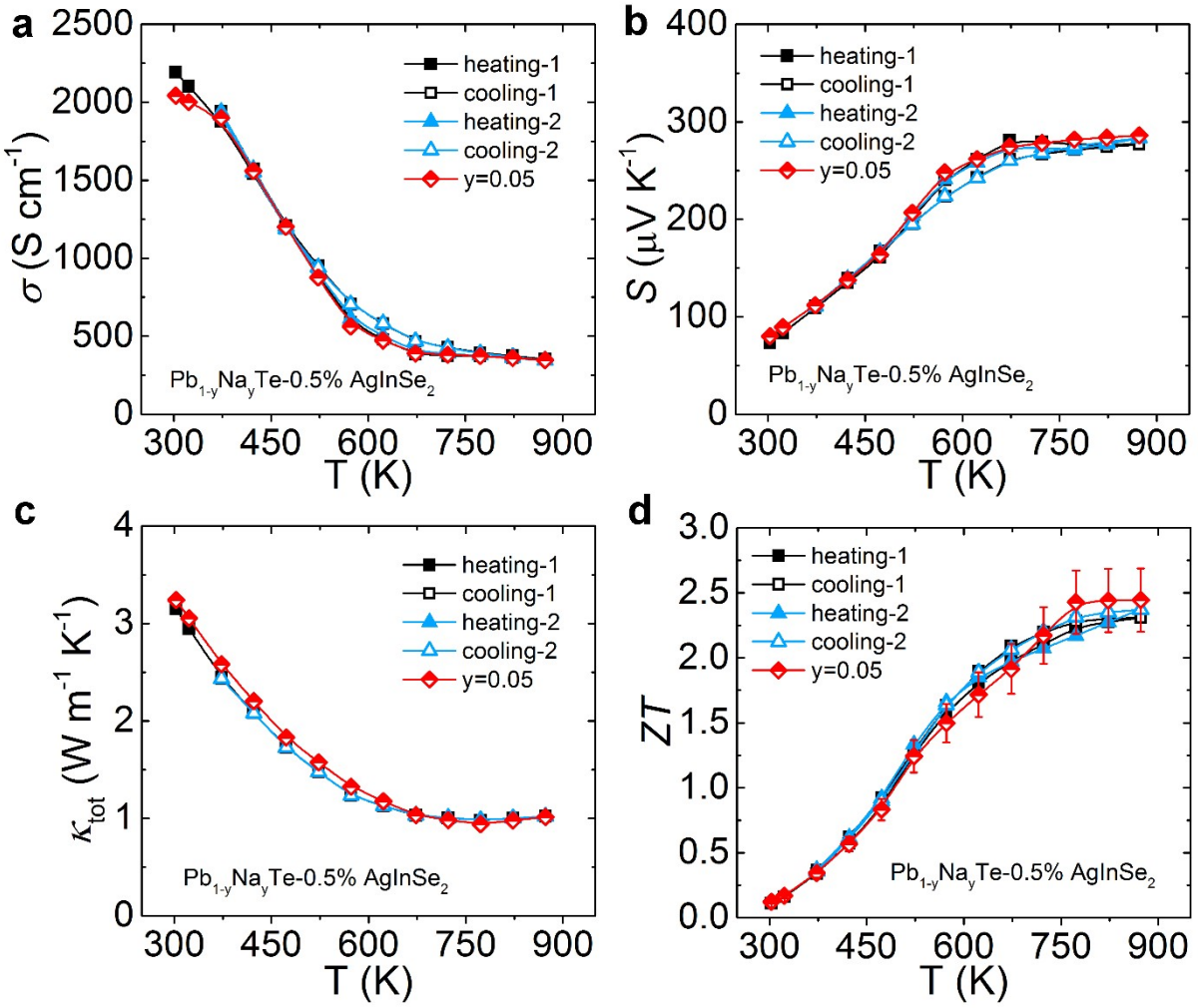

Figure S10. Temperature-dependent (a) electrical conductivity, (b) Seebeck coefficient, (c) total thermal conductivity and (d) figure-of-merit *ZT* for $Pb_{0.95}Na_{0.05}Te$ - 0.5% $AgInSe_2$. The heating and cooling data show a good repeatable, indicating that the sample is stable. The *ZT* is reproducible considering its uncertainty.

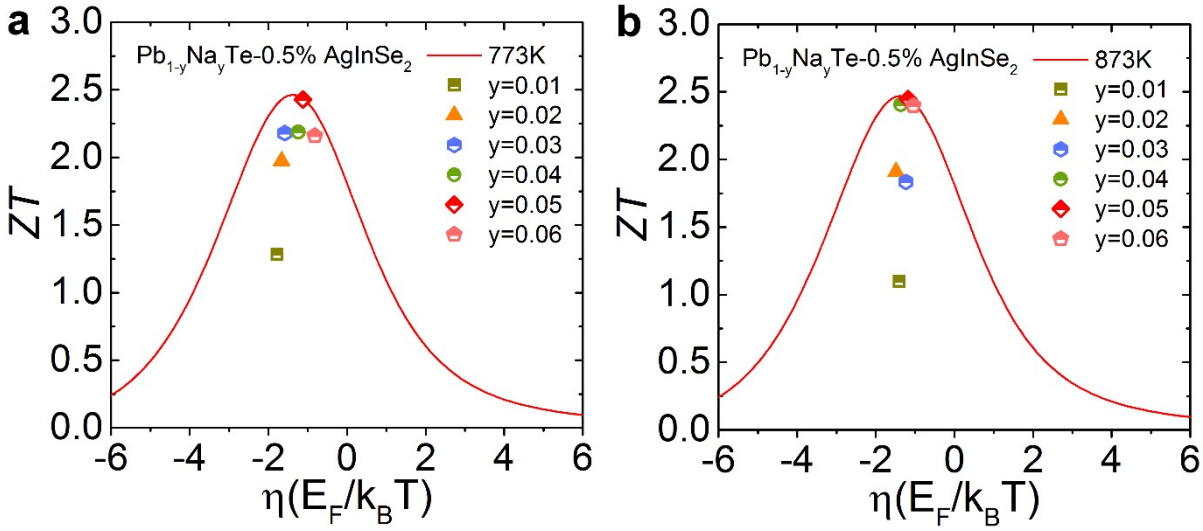

Figure S11. The figure-of-merit *ZT* as a function of reduced Fermi level at (a) 773K and (b) 873 K, respectively, for $Pb_{1-y}Na_yTe$ - 0.5% $AgInSe_2$. The dots show the experimental results and the red solid line represents the calculation.

Table S1. The coordination environment around Se assuming that Se occupies the Te site in PbTe matrix.

Shell	Coordination atom	Coordination number	Distance (Å)
1	Pb	6	3.22
2	Te	12	4.55
3	Pb	8	5.57
4	Te	6	6.44
5	Pb	24	7.19
6	Te	24	7.88
7	Te	12	9.11
8	Pb	30	9.65

References

[1] B. Ravel, Newville, M., *J. Synchrotron Rad.* **2005**, 12, 537.
[2] R. C. A. J.J. Rehr, *Rev. Mod. Phys.* **2000**, 72, 621.
[3] J. J. Rehr, J. J. Kas, F. D. Vila, M. P. Prange, K. Jorissen, *Phys. Chem. Chem. Phys.* **2010**, 12, 5503.
[4] A. F. May, G. J. Snyder, *CRC Press: Boca Raton, FL* **2012**, Vol. 1, pp 231.
[5] S. D. Kang, Snyder G. J., *arXiv:1710.06896 [cond-mat.mtrl-sci]* **2017**.
[6] L. M. Rogers, *Br. J. Appl. Phys.* **1967**, 18, 1227.
[7] S. V. Airapetyants, M. N. Vinograd, I. N. Dubrovsk, N. V. Kolomoet, I. M. Rudnik, *Soviet Physics Solid State* **1966**, 8, 1069.
[8] Y. Pei, X. Shi, A. LaLonde, H. Wang, L. Chen, G. J. Snyder, *Nature* **2011**, 473, 66.
[9] Y. I. Ravich, B. A. Efimova, I. A. Smirnov, *(Plenum Press, 1970)*.
[10] P. Jood, J. P. Male, S. Anand, Y. Matsushita, Y. Takagiwa, M. G. Kanatzidis, G. J. Snyder, M. Ohta, *J. Am. Chem. Soc.* **2020**, 142, 15464.
[11] R. N. Tauber, A. A. Machonis, I. B. Cadoff, *J. Appl. Phys.* **1966**, 37, 4855.